SHALLOW AND DEEP FRESH IMPACT CRATERS IN HESPERIA PLANUM, MARS

PETER J. MOUGINIS-MARK* and JOAN N. HAYASHI

Planetary Geosciences, Department of Geology and Geophysics, School of Ocean and Earth Science and Technology, University of Hawaii, Honolulu, HI, U.S.A.

(Received 11 June, 1992; revised 24 August, 1992)

Abstract. The depths of 109 impact craters ~2–16 km in diameter, located on the ridged plains materials of Hesperia Planum, Mars, have been measured from their shadow lengths using digital Viking Orbiter images (orbit numbers 417S–419S) and the PICS computer software. On the basis of their pristine morphology (very fresh lobate ejecta blankets, well preserved rim crests, and lack of superposed impact craters), 57 of these craters have been selected for detailed analysis of their spatial distribution and geometry. We find that south of 30° S, craters <6.0 km in diameter are markedly shallower than similar-sized craters equatorward of this latitude. No comparable relationship is observed for morphologically fresh craters >6.0 km diameter. We also find that two populations exist for older craters <6.0 km diameter. When craters that lack ejecta blankets are grouped on the basis of depth/diameter ratio, the deeper craters also typically lie equatorward of 30° S. We interpret the spatial variation in crater depth/diameter ratios as most likely due to a poleward increase in volatiles within the top 400 m of the surface at the times these craters were formed.

Introduction

Meteorite impact craters reveal important information on the near-surface stratigraphy of a planet. Because materials are ejected from depths ranging from 0.05–0.2 of the crater diameter (cf., Stoffler *et al.*, 1975; Hörtz *et al.*, 1983), it is possible to investigate the target stratigraphy at various depths via the analysis of the ejecta blankets and interiors of craters of different diameters (cf., Pieters, 1982). For Mars, this approach has been proposed as a useful method to study spatial variations in such attributes as the distribution of sub-surface volatiles (Mouginis-Mark, 1979; Barlow and Bradley, 1990) and heat flow (Boyce, 1979).

To date, investigations of Martian craters have primarily relied on geomorphic comparisons of ejecta deposits and the frequency of occurrence of interior features such as central peaks, central pits and terraces (Wood *et al.*, 1978; Mouginis-Mark, 1979; Pike, 1980). One early investigation (Cintala and Mouginis-Mark, 1980) that used shadow length measurements to obtain crater geometries offered promise for the quantitative comparison of fresh craters at different places on Mars. From their global study of 172 fresh Martian craters in the diameter range 0.7–80.0 km, Cintala and Mouginis-Mark (1980) believed that they could identify the modifying influence of a volatile layer that preferentially influenced crater depths for the diameter range ~3.0–5.0 km. Here we extend this type of study of

* *Present Address:* Planetary Geosciences, 2525 Correa Road, Honolulu, Hawaii 96822.

Earth, Moon, and Planets **61**: 1–20, 1993.

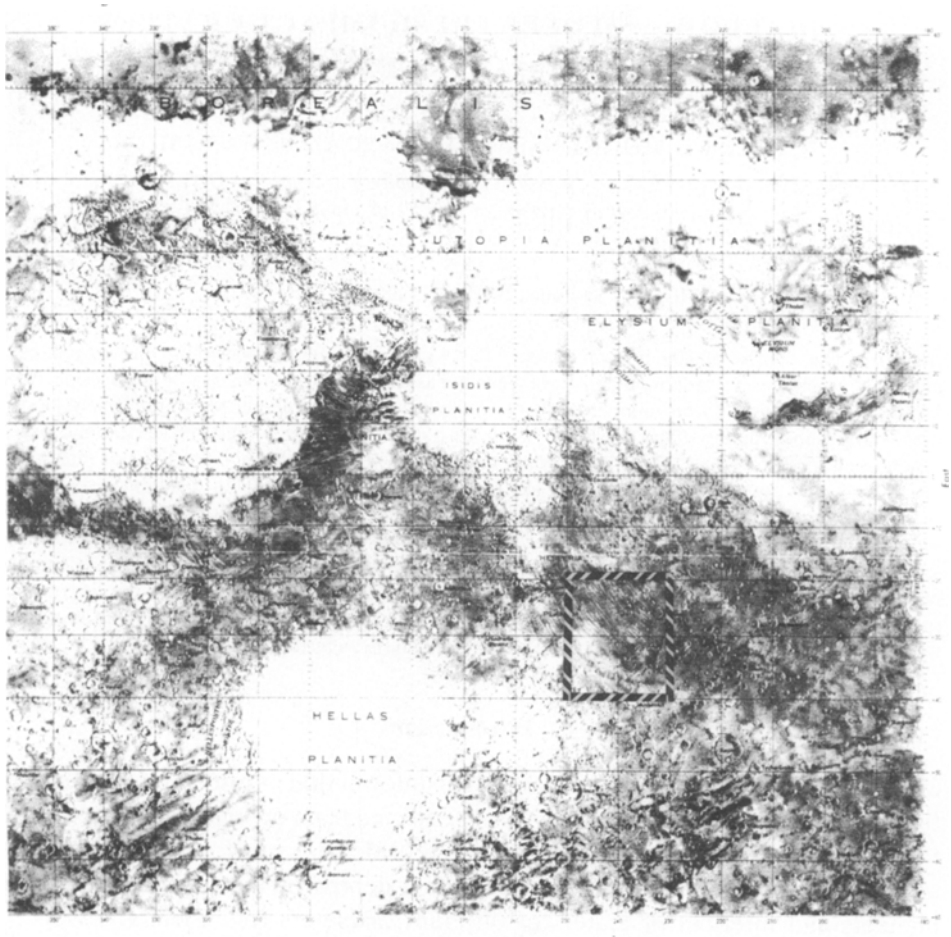

Fig. 1. Location map of the eastern portion of Mars, showing the area of Hesperia Planum included in this investigation.

crater geometry by concentrating on craters formed on the ridged plains materials of Hesperia Planum, Mars (~23–38° S, 233–248° W; Figure 1).

The origin and thickness of the ridged plains materials within Hesperia Planum (and other areas of Mars where this geological unit occurs) can be inferred from the unit's morphology and similarity with lunar landscapes. The Martian ridged plains are characterized by broad planar surfaces, rare lobate deposits, and long, parallel, linear to sinuous mare-type (wrinkle) ridges that are typically spaced about 30 to 70 km apart (Figure 2). Because of their similarity to the lunar maria, it is likely that these materials comprise a series of flood lavas that partially infilled topographic depressions within the Martian highlands (Greeley and Guest, 1987). Measurements of impact crater diameter and the heights of partially buried crater rims provide estimates that the lava flows within Hesperia Planum are between

Fig. 2. Example of the ridged plains within Hesperia Planum, showing several fresh impact craters. The diameter of the largest crater is 9.03 km and, together with craters labeled "A", has a sufficiently fresh appearing ejecta blanket to be included within the class of "pristine" craters in this analysis. The two craters labeled "B" were not included in this pristine category because they lack complete ejecta blankets, but they were included in subsequent studies of other deep craters (see Figure 9). Viking Orbiter image 418S39, centered at 28.56° S, 240.94° W. Image width is 95 km.

200–400 m thick (De Hon, 1985). However, we recognize that the physical properties of the buried terrain are unknown, and that it is not possible to identify the specific stratigraphy of the ridged plains materials. Furthermore, the ability of the ridge plains materials to store volatiles cannot be estimated with regard to how these volatiles may have affected the cratering process by influencing crater geometry or ejecta morphology (cf., Kieffer and Simonds, 1980).

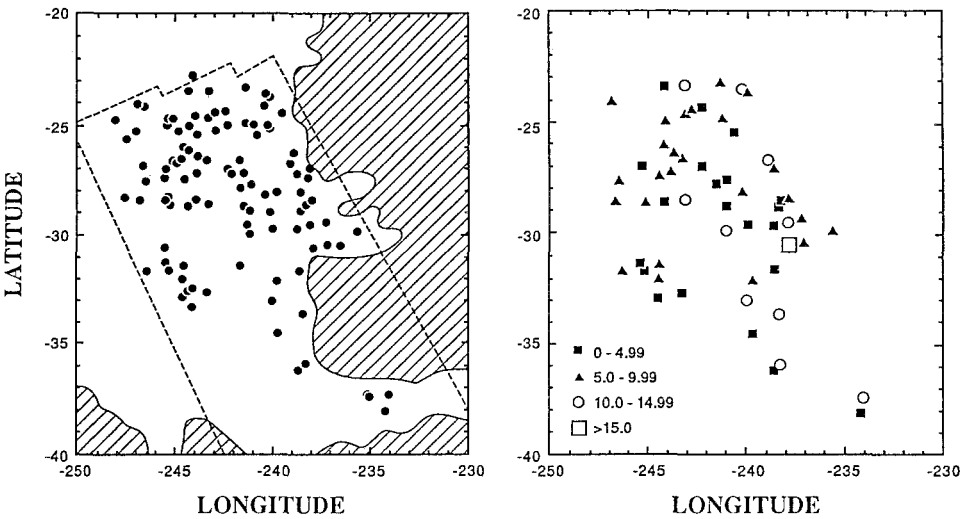

Fig. 3. Locations of all the impact craters that were measured in this analysis. (A) (left) includes all craters measured here; (B) (right) shows the distribution of fresh craters with well preserved ejecta blankets. Crater populations are subdivided into four categories, corresponding to diameter ranges <5 km, 5.0–9.99 km, 10.0–14.99 km and >15.0 km. Stippled area marks the edge of the cratered terrain to the east of the ridged plains, dotted line denotes area of coverage from Orbits 417–419S of Viking Orbiter 1.

New Data: Depth/Diameter Relationships

Shadow length measurements of 109 crater depths were made from digital versions of Viking Orbiter images obtained from orbits 417° S, 418° S and 419° S. Details of our measurement technique and possible errors are given in the Appendix. These Viking Orbiter images provide an unusually constant range of illumination geometries (incidence angle = 63–80°) and spatial resolution (88–96 m/pixel) for a large geographic area. To our knowledge, this represents the best data set that exists for the quantitative analysis of the ridged plains materials on Mars. Our sample contains craters in the diameter range 1.97–15.44 km (Figure 3). Of these craters, 57 are morphologically very fresh (Table I) and show the morphological characteristics previously used as evidence of subsurface volatiles (Carr *et al.*, 1977; Mouginis-Mark, 1979). The craters possess complete rims, well preserved ejecta blankets that completely surround the parent crater, have radial striations upon the ejecta lobes or sharp distal ramparts, and have no superposed impact craters (cf., Pike, 1980; Mouginis-Mark, 1981). It is these 57 craters that we interpret to be the youngest and least modified craters in this part of Hesperia Planum.

A comparison of the morphology of each of these 57 craters as a function of its size and location does not give any indication of a regional trend in target properties. For example, Wood *et al.* (1978) have suggested that craters with central pits mark the locations where volatiles were close to the surface at the time of impact.

TABLE I

Geometry of all fresh craters measured in this analysis. The technique for measuring crater diameter and depth is described in the Appendix along with the method for determining the associated errors

Latitude	Longitude	Dia. (km)	Dia. error	Depth (km)	Depth error	Depth/dia.	*d/D* error
−27.00	−242.30	2.44	0.13	0.55	0.06	0.225	0.036
−27.00	−245.40	2.64	0.10	0.49	0.06	0.185	0.030
−32.90	−244.60	2.89	0.09	0.34	0.05	0.118	0.020
−36.20	−238.60	2.95	0.08	0.32	0.03	0.108	0.015
−38.10	−234.30	2.97	0.06	0.27	0.02	0.090	0.010
−31.60	−238.60	3.10	0.11	0.53	0.04	0.171	0.020
−31.60	−245.20	3.28	0.10	0.30	0.05	0.092	0.018
−29.60	−238.70	3.31	0.15	0.38	0.05	0.116	0.021
−27.60	−241.10	3.50	0.22	0.74	0.06	0.211	0.029
−25.40	−240.70	3.79	0.07	0.67	0.07	0.177	0.021
−34.50	−239.70	3.84	0.10	0.32	0.04	0.083	0.012
−27.80	−241.60	3.93	0.13	0.48	0.06	0.123	0.018
−29.60	−240.00	3.96	0.12	0.69	0.05	0.175	0.019
−28.80	−241.10	4.04	0.06	0.70	0.05	0.172	0.016
−28.50	−238.30	4.22	0.13	0.78	0.05	0.186	0.019
−28.60	−244.30	4.28	0.16	0.51	0.06	0.120	0.017
−23.40	−244.30	4.33	0.21	0.77	0.07	0.178	0.025
−32.70	−243.30	4.69	0.10	0.36	0.05	0.077	0.011
−24.30	−242.40	4.73	0.15	0.62	0.07	0.131	0.018
−31.20	−245.40	4.80	0.35	0.41	0.05	0.086	0.017
−28.80	−238.50	4.97	0.06	0.46	0.05	0.094	0.012
−24.90	−244.20	5 01	0.19	0.83	0.07	0.165	0.020
−31.60	−246.30	5.20	0.25	0.73	0.05	0.141	0.017
−29.30	−237.30	5.61	0.21	0.71	0.05	0.126	0.014
−28.40	−238.00	5.67	0.06	0.78	0.05	0.137	0.011
−23.90	−246.90	5.86	0.35	0.83	0.07	0.142	0.021
−24.80	−241.30	5.98	0.14	0.88	0.07	0.147	0.015
−32.00	−244.50	6.17	0.26	0.77	0.05	0.125	0.013
−24.40	−242.90	6.31	0.26	0.67	0.07	0.106	0.015
−26.00	−244.30	6.35	0.31	0.84	0.07	0.133	0.017
−31.40	−244.50	6.36	0.16	0.57	0.05	0.089	0.010
−27.20	−243.90	6.73	0.18	0.85	0.06	0.127	0.013
−24.60	−243.20	6.78	0.23	0.67	0.07	0.099	0.013
−23.60	−240.10	6.99	0.09	0.95	0.07	0.136	0.012
−27.50	−246.50	7.00	0.35	0.66	0.06	0.095	0.014
−27.10	−238.70	7.11	0.50	0.73	0.06	0.103	0.015
−26.40	−243.80	7.32	0.35	1.07	0.06	0.146	0.016
−26.60	−243.30	7.54	0.43	0.80	0.06	0.106	0.014
−28.40	−246.70	7.64	0.12	0.85	0.06	0.111	0.009
−32.10	−239.70	7.80	0.21	0.67	0.04	0.086	0.008
−30.40	−237.20	7.94	0.11	1.24	0.05	0.156	0.008
−23.20	−241.40	8.32	0.38	0.49	0.07	0.059	0.012
−29.80	−235.70	8.99	0.17	1.11	0.05	0.124	0.007
−28.10	−240.30	9.04	0.23	0.84	0.05	0.093	0.008
−27.40	−244.50	9.28	0.32	0.98	0.06	0.105	0.010
−28.60	−245.20	9.57	0.13	0.76	0.06	0.079	0.007
−37.40	−234.10	10.51	0.29	0.71	0.02	0.067	0.004
−29.50	−238.00	10.62	0.25	1.00	0.05	0.094	0.007
−35.90	−238.30	10.84	0.43	0.70	0.03	0.065	0.006

TABLE I. Continued

Latitude	Longitude	Dia. (km)	Dia. error	Depth (km)	Depth error	Depth/dia.	d/D error
−33.60	−238.40	11.64	0.34	1.22	0.04	0.105	0.006
−23.50	−240.30	13.46	0.27	1.09	0.07	0.081	0.007
−29.90	−241.10	14.22	0.83	0.97	0.05	0.068	0.008
−28.50	−243.20	14.24	0.66	1.27	0.06	0.089	0.008
−33.00	−240.00	14.28	0.56	0.37	0.04	0.026	0.004
−23.30	−243.20	14.45	0.34	0.90	0.07	0.062	0.006
−26.70	−239.00	14.95	0.81	1.23	0.06	0.082	0.008
−30.50	−237.90	15.44	0.75	1.32	0.05	0.085	0.007

Nine of our youngest and least modified craters (6.78–15.44 km in diameter) have central pits, but these craters are found between 23.50–30.40° S. Craters with central peaks have diameters from 5.98–14.28 km, and are found between 24.40–35.90° S. Were the presence of central pits to be diagnostic of nearsurface volatiles, we find it surprising that the distribution of these two types of crater interior morphologies overlap considerably. Similarly, no systematic distributions of other features within craters are observed. Five bowl-shaped craters (2.44–4.04 km diameter) are found between latitudes 27.00–31.60° S, while flat floored crater in a similar size range (2.89–4.22 km diameter) are found between 25.40–38.10° S. Scalloped walls (Wood *et al.*, 1978) are first seen in a crater that is 4.80 km diameter at 31.20° S, and terraces are first seen in a 8.32 km diameter crater at 23.20° S.

For many of our crater geometry measurements, but particularly crater rim heights, the shadow lengths (and, hence, heights and depths) were calculated from only a few (<10) pixels. As described in the Appendix, we take 1.5 pixels as the accuracy to which we can measure shadow lengths (Robinson, 1990), which translates to ~140 m on the Martian surface. For high-sun (INA <70°) images, we thus have an uncertainty of ±20–70 m in our depth and rim height measurements. For crater depths, this amounts to 5–15%, but for rim heights this error may be as large as 30%. When using the rim height to infer the depth of excavation (i.e., the depth below the target's original surface), caution should be exercised in interpreting our data because we found it difficult to locate the exact edge of the shadow. It is also possible that we measured the height of the rim crest above the ejecta blanket rather than the height of the crater rim above Hesperia Planum.

Cintala and Mouginis-Mark (1980) inferred that the role of volatiles within the target material had a significant influence on the depth/diameter (d/D) relationship of craters smaller than 10 km diameter. We present our own measurements of d/D for the 57 pristine Hesperia Planum craters (Figure 4). Significant scatter exists in the depth for a crater of any diameter, but particularly for craters <5 km. We have therefore divided the population of small fresh craters into two categories, denoted as "shallow" and "deep" (Figure 5a). This subdivision is not a statistical separation of classes, but assumes that if all aspects of the cratering process were

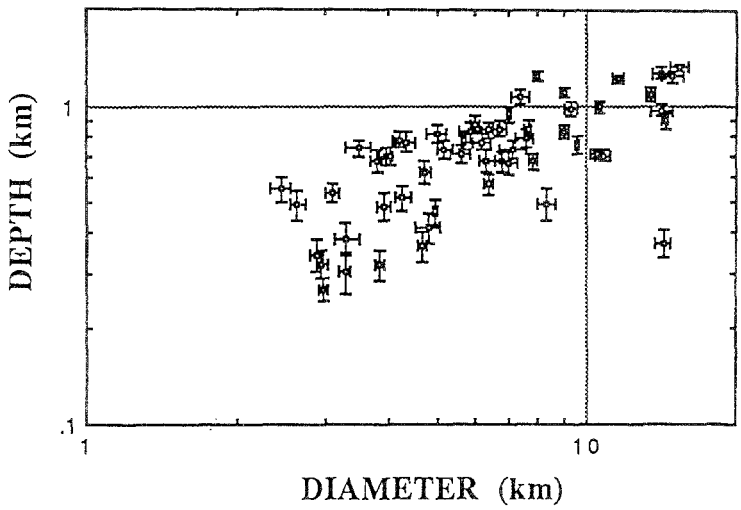

Fig. 4. Depth vs. diameter plot for the 57 fresh Hesperia Planum impact crater investigated.

the same (e.g., target stratigraphy, impact energy, bolide type) then craters of equal diameter should have equal depth (Mouginis-Mark, 1981). Since our crater geometry measurements show that this is not the case, we interpret the data to mean that at least one aspect of the impact events was varying. In a quantitative sense, the "deep" craters are 50–100% deeper than the "shallow" fresh craters of the same diameter.

In our own earlier analysis of a subset of these data (Hayashi-Smith and Mouginis-Mark, 1990) we did not investigate the spatial variability of craters with any specific d/D value, and drew what we now believe to be the incorrect conclusion that there is no general trend in crater morphometry that could be related to target material properties. Once the spatial distribution of these craters is investigated (Figure 5b), the differences are apparent. "Deep" craters are generally located in the northern part of Hesperia Planum, while "shallow" craters are more commonly found in the south. This relationship is non-exclusive (Figure 5b), but the pattern appears to be real. We will discuss the possible physical situation that has led to the distribution of these two crater types in the discussion section.

We have also investigated the possible existence of the equivalent "deep" and "shallow" craters for fresh craters larger than 6 km in diameter. From the d/D plot for these larger craters (Figure 4), it is less clear that two populations of large craters exist. As for the smaller craters, we have separated craters that have the highest d/D ratios from those with lower ratios but the same diameter (Figure 6a). When the spatial distribution of these two classes of large craters are compared (Figure 6b), we see no uniform trend in locations. From Figure 6b we infer that whatever property of Hesperia Planum is responsible for affecting craters smaller than 6 km diameter, this attribute does not affect larger craters.

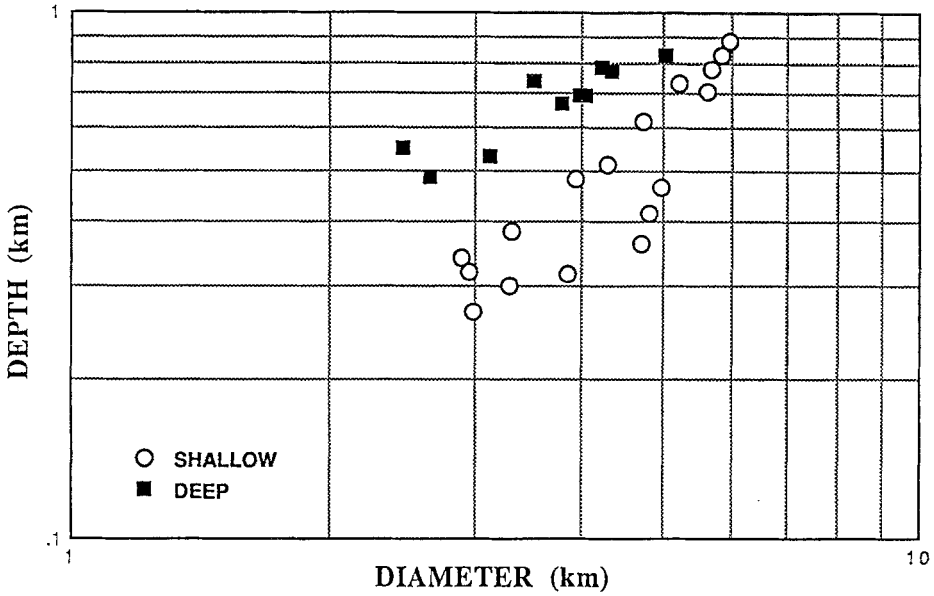

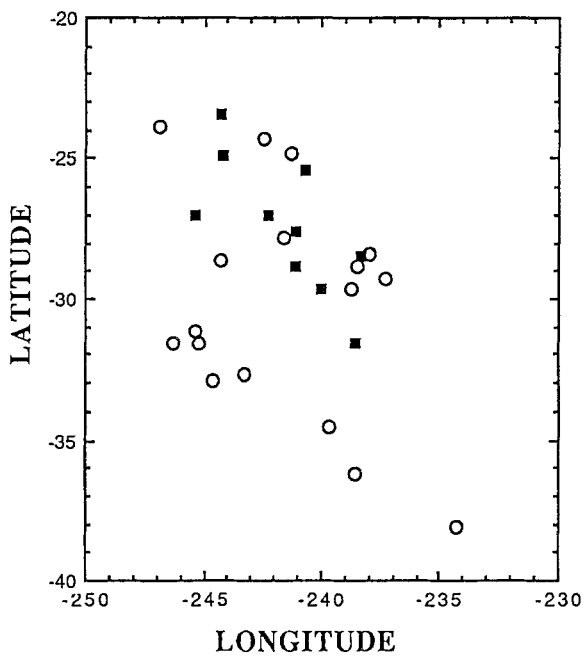

Fig. 5. (A) (Top) Enlargement of depth vs. diameter plot presented in Figure 4, showing craters smaller than 6.0 km in diameter. Crater population has been subdivided into two classes of craters that appear to be "deep" or "shallow" for each diameter. (B) (Bottom) Spatial distribution of the small fresh craters in Figure 5a. The same symbols denote "deep" or "shallow" craters. Note that shallow craters are preferentially located poleward of 30° S, while "deep" craters are predominately equatorward of this latitude.

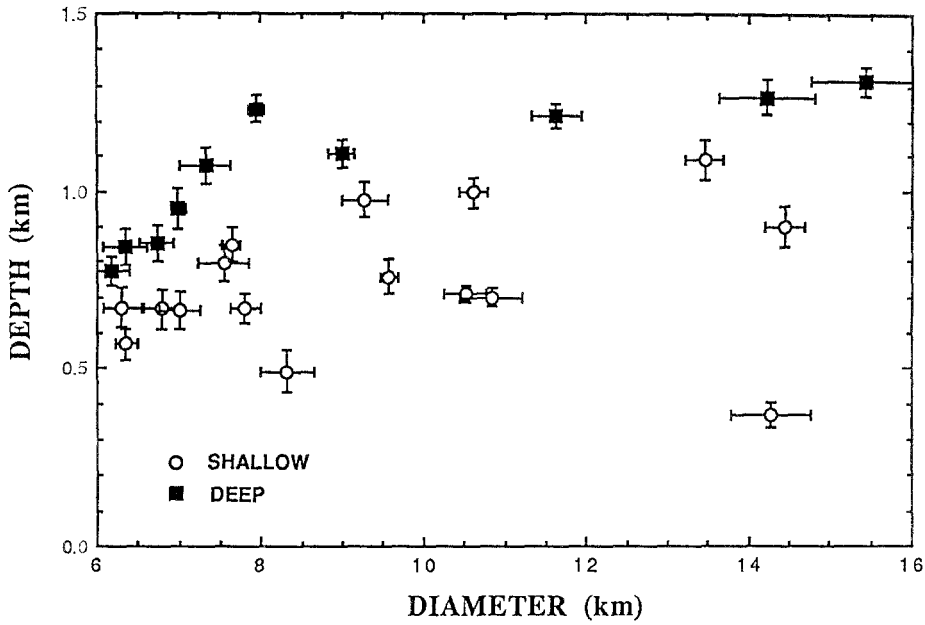

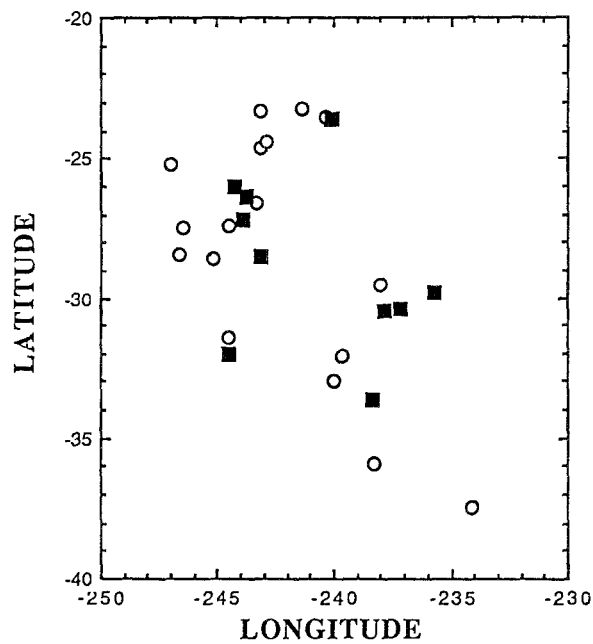

Fig. 6. (A) (Top) Depth vs. diameter plot of pristine craters larger than 6.0 km in diameter. Note that the scales used here are linear to expand the scatter of data points. Craters with the largest d/D ratio are called "deep" craters, while smaller d/D values are associated with "shallow" craters. Derivation of error bars is discussed in the Appendix. (B) (Bottom) Spatial distribution of deep and shallow fresh craters in the diameter range 6.0–15.44 km, as identified in Figure 9a. Note that there does not appear to be any systematic pattern to the distribution of these two classes of crater, suggesting that the excavation depth exceeds the thickness of the near-surface volatile layer.

Discussion

The earlier premise (Cintala and Mouginis-Mark, 1980) was that sub-surface volatiles had a variable distribution with depth. A second look at these data that one of us (PMM) helped collect in Cintala and Mouginis-Mark (1980) reveals that many of the craters included in the earlier study would not have been considered sufficiently fresh, or have the appropriate image data available for digital measurements, for inclusion in the current Hesperia Planum study. For example, Cintala and Mouginis-Mark (1980) included craters from many geographic areas on Mars in their study, and did not consider possible spatial differences in target rock (Pike, 1980). Only 15 of the 172 craters measured by Cintala and Mouginis-Mark (1980) are located on ridged plains materials, and three of these craters lack ejecta blankets. Image quality must also be suspect for the Cintala and Mouginis-Mark (1980) analysis. Data were collected by digitizing crater rim diameters and shadow length from 3.5 × 4.0 inch hard-copy NSSDC SCR prints that were batch processed to enhance contrast. While the illumination geometry was constrained to only include images with incidence angles between 65–90, with the computer capabilities of that time we question our earlier ability to measure precisely crater dimensions on these prints. Furthermore the spatial resolution of the images had a wide range, from 15–50 m/pixel, so the errors for each measurement were also highly variable.

Despite the potential limitations of the analysis methods of Cintala and Mouginis-Mark (1980), the current measurements of d/D (Figure 5) support their idea of a variation in crater geometry for craters <6.0 km diameter. We can further investigate this spatial variation via a comparison of d/D vs. latitude (Figure 7). Prominent in Figure 7 is the general increase in d/D from high latitudes to low latitudes, with values typically less than 0.1 poleward of 32° S and often greater than 0.15 equatorward of 30° S. Figure 7 also shows that this latitudinal variation in large d/D values is, to a first approximation, related to the size of the crater. There is a cluster of 15 craters (denoted by the dashed area in Figure 7) that includes 12 craters <6 km diameter that have large d/D values for their latitude. Although the sample size is small, a trend appears to exist such that small craters poleward of ~32° S are only ~50–70% as deep as craters with a similar diameter that lie closer to the equator than ~30° S.

We now consider two mechanisms that may explain this poleward shallowing of fresh craters; (1) spatial variations in the thickness of the lava flows that comprise the surface material of Hesperia Planum, and (2) latitudinal variations in volatiles in the near-surface (top 500 m?) of the target. The thickness of the Hesperia Planum lava flows is believed to vary from more than 400 m in the northwest of our study area to less than 200 m to the southeast (De Hon, 1985). It is likely that the underlying materials comprise heavily cratered terrain similar to the materials that outcrop around the perimeter of Hesperia Planum. In order for target properties to affect the geometry of the crater, we assume that the crater

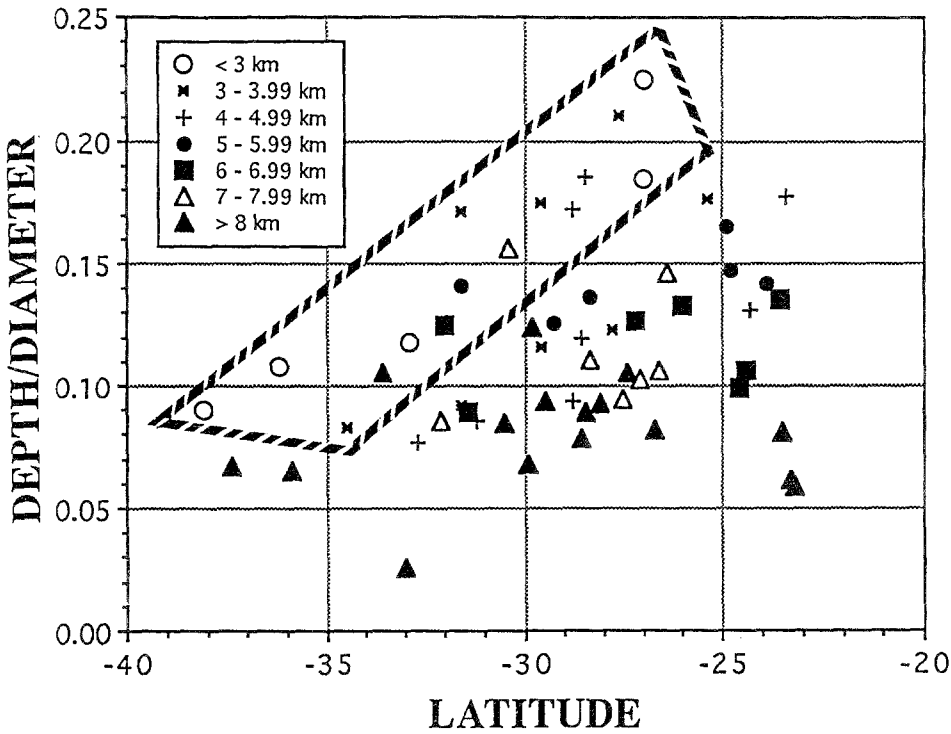

Fig. 7. Distribution of depth/diameter (d/D) ratios for all 57 fresh craters as a function of latitude. The dashed area denotes a cluster of 15 craters, 12 of which are <6.0 km diameter, that have unusually large d/D values for their latitude. Note that all fresh craters <3 km diameter are included in this cluster, and that the d/D values of these craters show a marked decrease with increasing latitude.

cavity must be excavated to the depth of the interface between the lava flows and the underlying materials. Note that we are primarily interested in the order of magnitude of the thickness of these plains materials, and do not need to know the values to better than an accuracy of ~100 m. For nine of the craters that we measured, it was possible to obtain estimates of the height of the crater rim above the surrounding ejecta blanket (Table II), even though in several instances this required measuring shadow lengths that might be only a few (3–6) pixels in size. These rim height measurements are assumed to be the same as the height above the preexisting surface, although it is possible that structural uplift of the rim, or variations in ejecta thickness upon which the shadow of the rim crest was measured, may complicate this relationship. Given these crater rim heights and the depths of the craters, the depth to which the fresh craters excavated the target material can be computed by subtracting the rim height from the crater depth (Figure 8). From the excavation d/D relationship, craters larger than ~2 km diameter should excavate to a depth of 200 m, and a crater ~5 km in diameter should excavate to a depth of 400 m. Thus if plains thicknesses were to control

TABLE II

Rim height measurements for the 9 fresh craters where a rim shadow could be measured. "RH" refers to rim height. The excavation depth ("EXCAV.") is the inferred depth of the crater below the level of the preexisting terrain

Latitude	Longitude	Dia. (km)	Rim ht (km)	RH error	Excav. (km)
−38.10	−234.30	2.97	0.11	0.02	0.156
−28.80	−241.10	4.04	0.17	0.05	0.522
−28.40	−246.70	7.64	0.40	0.06	0.445
−37.40	−234.10	10.51	0.15	0.02	0.559
−33.60	−238.40	11.64	0.44	0.04	0.782
−23.50	−240.30	13.46	0.33	0.07	0.755
−29.90	−241.10	14.22	0.24	0.05	0.735
−26.70	−239.00	14.95	0.37	0.06	0.866
−30.50	−237.90	15.44	0.39	0.05	0.922

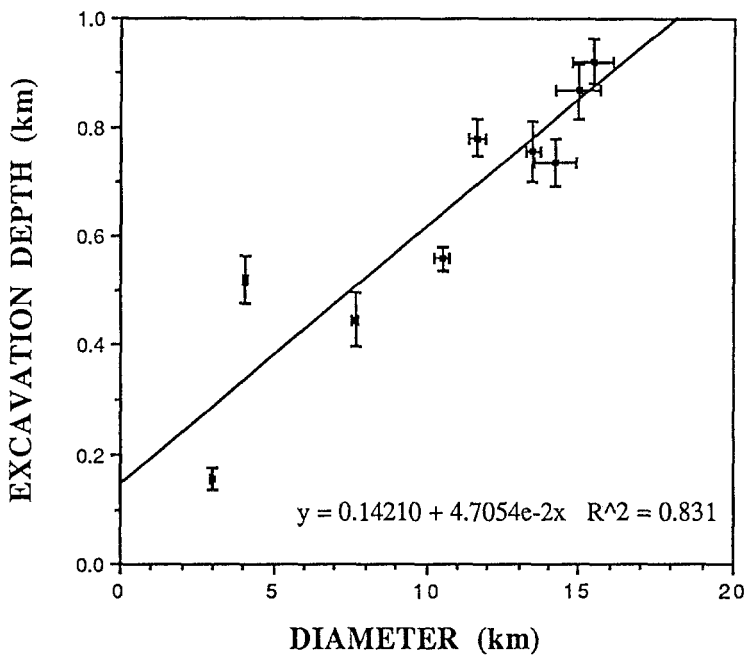

Fig. 8. Plot of crater diameter vs. "excavation depth" for nine fresh craters within Hesperia Planum for which rim heights could be measured. Excavation depth is calculated from the crater depth minus the rim height. Derivation of errors is discussed in the Appendix.

the crater geometry, one would expect to see a correlation between the map of plains thickness (De Hon, 1985) and the spatial distribution of depth/diameter ratios. We will return to consider this spatial distribution in the section below.

The alternative method for modifying small crater geometry in Hesperia Planum is one that involves a spatially-variable concentration of volatiles in the top few hundred meters of the target at the time that the craters were formed. This idea is not new, indeed it was the preferred mechanism proposed by Cintala and

Mouginis-Mark (1980) to explain the variations in crater depth/diameter ratios. Fanale (1976) and Fanale *et al.* (1986) have modeled the situation where volatiles were driven towards the poles over Martian history, and the trends revealed for the small craters (Figure 5) would support this poleward migration model. Our current analysis of the Hesperia Planum craters (Figure 5a) may also show that for craters <5 km in diameter, there is a gradual transition of volatiles within the target. In particular, if a spatial variation in volatiles were the controlling factor in influencing the crater geometry, then we would expect to see a relationship between the crater's latitude and d/D. From Figure 8, we infer that a volatile layer had to be at a depth of less than 400 m at the time of impact to influence crater geometry. However, we caution the reader that this depth is also very close to the one inferred to be the thickness of the ridged plains materials (De Hon, 1985), and so our interpretation may be dominated by the stratigraphy of the target.

A further test of the latitudinal variation in d/D is to consider the geometry of other small craters in Hesperia Planum that have well preserved rim crests but lack the continuous ejecta blankets that were a feature of the pristine craters (Figure 2). These craters are probably somewhat older than the examples included in Table I, since the ejecta blankets have been buried or removed by erosion. Unlike the craters included in our sample of 57 craters, the lack of the lobate, fluidized, ejecta blankets for this second set removes one of the main morphological indicators that independently suggest that volatiles were present in the target at the time of the impact. However, this second set of craters are not so old that the rim crests have experienced any appreciable erosion, so that their interior geometry may still provide useful information on the cratering process. We have measured the depth and diameter of 52 additional craters that fall into this category. This sample of craters can also be subdivided into those that have high and low d/D values (Figure 9a). When the spatial distribution of these craters without ejecta blankets is investigated (Figure 9b), the same latitudinal variation can be seen as for the pristine craters. Craters with large d/D values are typically equatorward of 30° S, while low d/D craters are found at all latitudes. Our measurements of the 14 craters without lobate ejecta that are described as deep craters are presented in Table III.

Although a latitudinal variation in the distribution of craters may exist, we return to the possibility that target properties may instead be controlling the occurrence of these crater geometries. To investigate this possibility, we compare the spatial distribution of all the deep craters identified in Figures 5 and 9 to the inferred thickness variations of the ridged plains materials within Hesperia Planum (Figure 10). From inspection of De Hon's (1985) thickness map, the ridged plains at certain latitudes in this area are interpreted to vary from <200 m in the east to >400 m in the west. From Figure 10, it is apparent that all but two of the 24 craters with a large d/D value are equatorward of 30° S, but are formed in parts of Hesperia Planum that have estimated thicknesses between <200 to >400 m.

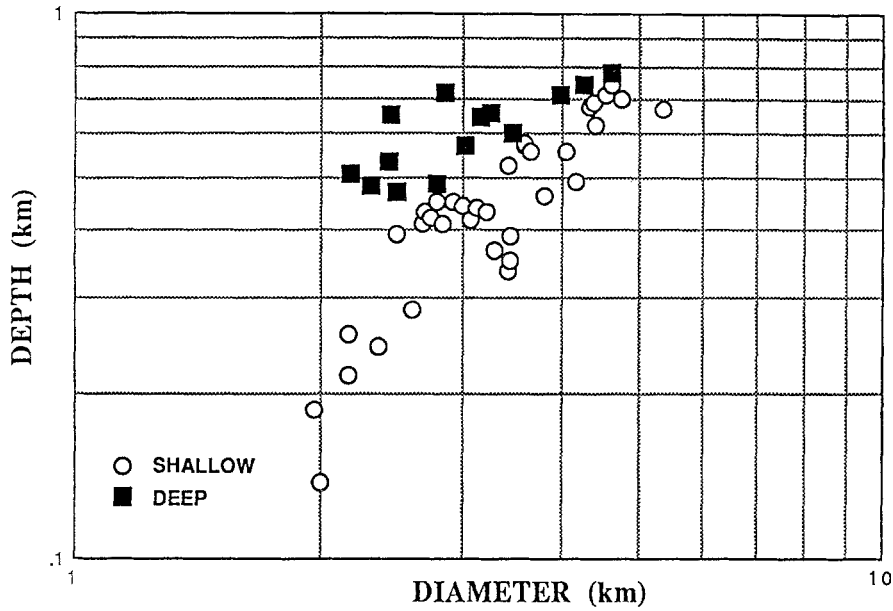

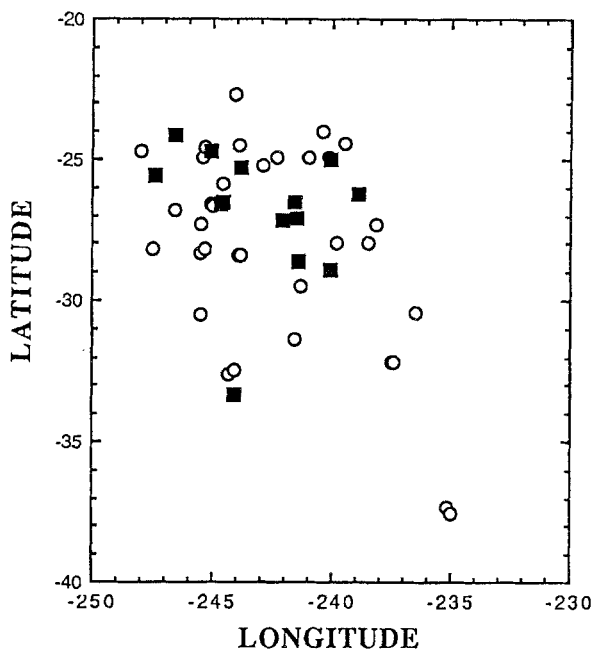

Fig. 9. (A) (Top) Depth vs. diameter plot of 48 craters that were measured here that do not have lobate ejecta blankets and are smaller than 6.0 km diameter. As with Figure 5a, these craters have been subdivided into two classes, "deep" and "shallow" for their respective diameters. (B) (Bottom) Spatial distribution of the 48 craters presented in Figure 9a. Note that a similar distribution to the one presented in Figure 5b is observed for the deep craters, which are preferentially found equatorward of 30° S.

TABLE III

Geometry of 14 deep craters that lack ejecta blankets. These craters are therefore inferred to be somewhat older than the sample given in Table I

Latitude	Longitude	Dia. (km)	Depth (km)	Depth/dia.
−24.10	−246.60	2.86	0.72	0.251
−33.30	−244.10	2.44	0.65	0.267
−24.70	−245.10	3.02	0.57	0.190
−26.50	−244.60	3.26	0.65	0.201
−26.60	−244.70	2.31	0.48	0.208
−26.50	−241.60	2.49	0.47	0.188
−27.20	−242.10	2.18	0.51	0.233
−27.10	−241.50	2.44	0.53	0.219
−25.00	−240.10	2.79	0.49	0.174
−26.20	−238.90	3.17	0.65	0.204
−28.60	−241.40	3.46	0.60	0.174
−25.30	−243.80	4.25	0.74	0.174
−28.90	−240.10	3.98	0.71	0.178
−25.60	−247.40	4.60	0.78	0.170

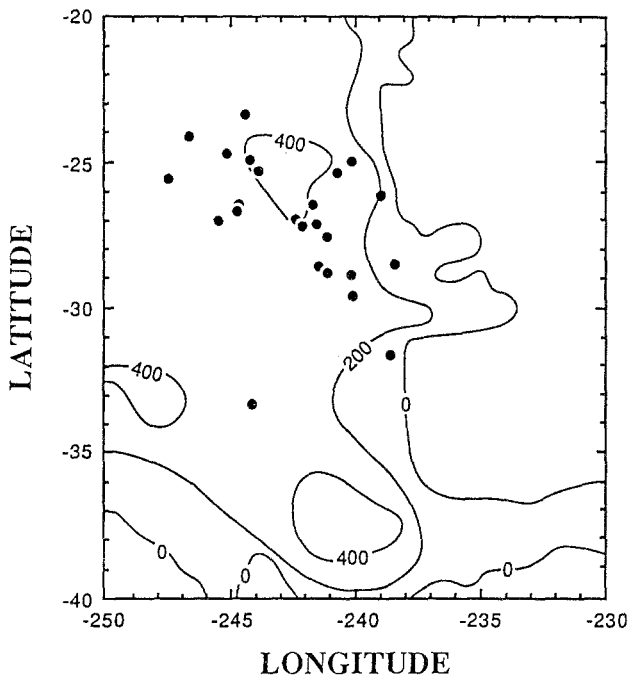

Fig. 10. Distribution of all "deep" craters presented in Figures 5 and 9. Superimposed on this distribution is the map of inferred lava flows thicknesses within Hesperia Planum, based on the partial burial of the rims of large craters (De Hon, 1985). Note that deep craters are found where the thickness of the flows is believed to vary from <200 m to >400 m, suggesting that substrate thickness is not a determining factor that influences the distribution of these small craters.

Thus, we believe that this east-west variation in plains thickness (which is probably the entire range of plains thicknesses within our study area) was not the primary physical characteristic of the target that caused some craters to be unusually deep or shallow. We therefore interpret the observed distribution in crater geometries to be due to spatial variations in volatiles at shallow depth, consistent with the model for the poleward migration of volatiles proposed by Fanale (1976).

Conclusions

We have used digital versions of Viking Orbiter images to develop the first quantitative data base of crater depths and diameters for a single geological unit on Mars. 109 craters between 1.97–15.44 km in diameter were included in this study, including 57 that appear to be pristine. Analysis of the d/D values has revealed that craters <6.0 km diameter were most likely affected by a latitudinally variable layer of volatiles. Craters at higher latitudes are shallower than craters of the same diameter that are closer to the equator. This relationship appears to be true both for craters with well preserved ejecta blankets and for deeper craters that lack ejecta but have well preserved rims. In each case, we believe that a decrease in volatiles within the target may account for this increase in d/D and, for the craters included in Table III, may be responsible for Martian craters that are more "lunar-like" and lack ejecta blankets. While we are unable to quantify the change in the amount or depth of burial of the volatiles, our observations add to the current body of observational evidence and numerical models which suggest that volatiles existed within the shallow Martian crust. Furthermore, these volatiles must have been present quite recently because they affected some of the freshest impact craters, which we infer to be quite young (<1 byrs?) due to the lack of erosion of their ejecta blankets and rim crests.

The Viking Orbiter data used here are particularly well suited to this form of digital analysis, due to their uniforrn spatial resolution, large area of coverage of a single geologic unit, and the small range of illumination geometries. Use of the digital Viking Orbiter data for other areas of Mars would be much more difficult, either because of variations in viewing geometry or in the diversity of terrain types imaged on a single orbit under similar lighting conditions. Nevertheless, measurements of a few d/D values for each lithologic unit may permit the qualitative inter-comparison of volatile concentrations based on the geometry of fresh meteorite craters. The depth of the largest crater with a high d/D ratio in any area could therefore define the maximum thickness of the volatile-depleted layer over the period when the craters formed. In the near future, our abilities to carry out such a regional comparison will be greatly improved, in as much as the Mars Observer Laser Altimeter (Zuber *et al.*, 1992) should permit the collection of a topographic data set that will be appropriate for investigating the global distribution of crater depths on Mars.

Acknowledgments

We thank Mark Robinson and Harold Garbeil for technical assistance in the measurement of the crater depths, and Phil Davis (U.S. Geological Survey, Flagstaff) for advice in the use of PICS software in Hawaii. Comments on an earlier version of this manuscript from an anonymous reviewer and Mark Robinson are also acknowledged. The research was supported by Grant NAGW-437 from NASA's Planetary Geology and Geophysics Program. This is Planetary Geosciences Contribution No. 720 and SOEST Publication No. 3142.

Appendix

Measurement of crater diameter: Crater depth/diameter measurements were made using digital versions of the Viking Orbiter images and the PICS image processing software. Typically, the average of three crater diameters was used for each crater, one diameter being measured in the same direction as the sun angle and two at about $\pm 45°$ to the solar azimuth. No correction was applied for variations in emission angle since this is not expected to introduce any appreciable error. In all cases, the rim crest of the crater was taken to be the point where there was a rapid variation in the data number (DN) values (in PICS this typically corresponded to a change of 3–5 times the variation observed for illuminated terrains). The rapid increase in DN values was also used to determine the edge of the shadow and, from simple trigonometry, the height of the crater rim. The 95% confidence level of the standard estimate of error (defined as 1.96 times the standard deviation of the measured values divided by the square root of the number of measurements) of these three diameter measurements is given as the error term (Table I).

Measurement of depth and rim height: The average resolution (in meters per pixel) of each frame and the lighting geometry at the crater center were used to convert measurements (obtained as the number of pixels on an image) into distances and shadow lengths and, hence, crater depths. Assuming all the error to

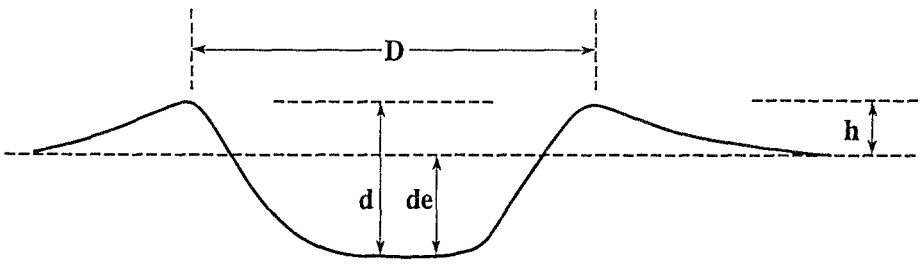

Fig. A1. Schematic of the dimensions of the craters measured here. "D" is the crater rim crest-to-rim crest diameter, "*d*" is crater depth, "*h*" is the height of the rim crest above the preexisting terrain, and "*de*" is the excavation depth.

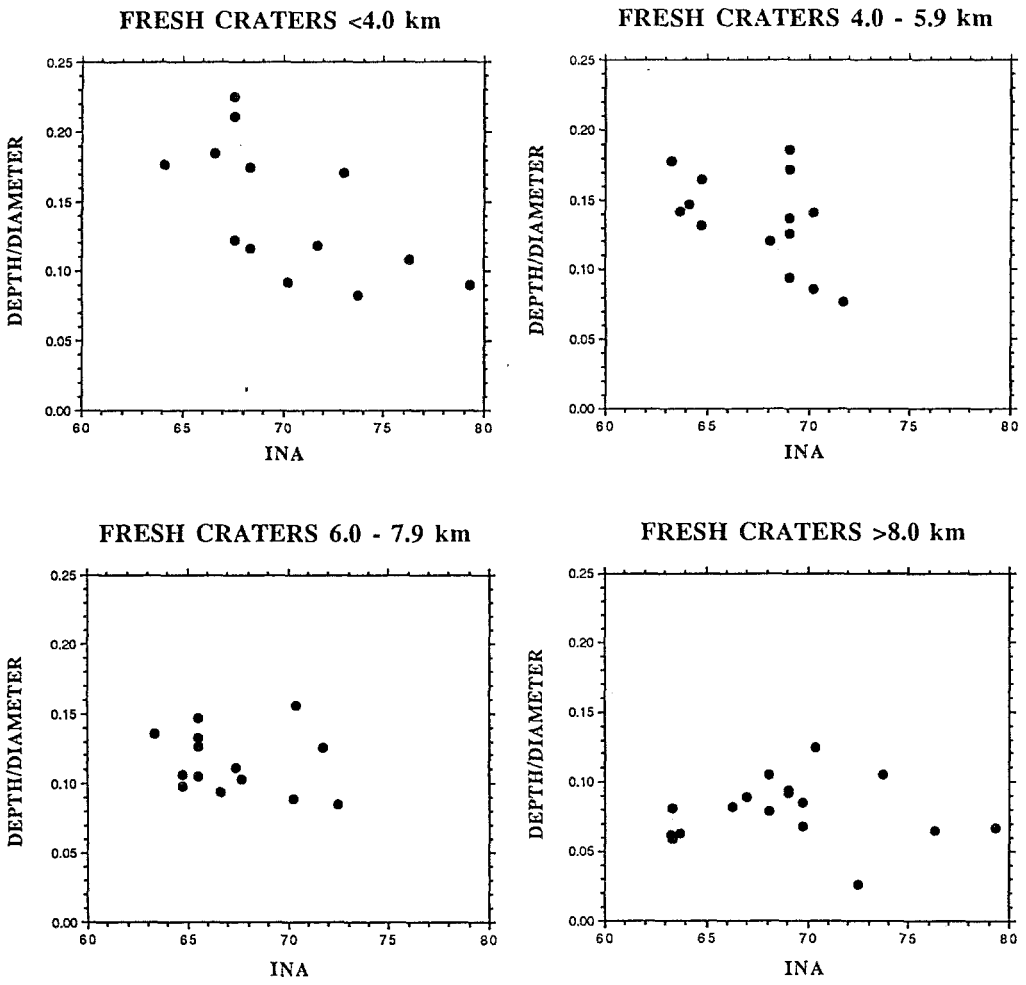

Fig. A2. The possible effects of variable illumination geometry on our ability to measure crater depths can be investigated via these four plots of d/D ratio versus incidence angle (INA) for different size craters. If there was a systematic bias against high-sun images (INA $< \sim 70°$) we would expect lower depths and, hence, smaller d/D values to be associated with high-sun images. In none of the four crater sizes (<4.0, 4.0–5.99, 6.0–7.99, and >8.0 km diameter) does this effect appear, and so we are confident that the shadow of the crater rim was indeed falling on the crater floor, rather than the inner wall.

be due to the determination of the shadow edge, errors for these depth measurements (Table I) were computed from (Robinson, 1990):

$$\tan(90\text{-INA}) * \text{average pixel resolution for frame} * 1.5 \text{ pixels},$$

where INA is the solar incidence angle at the center of the crater. For a few of the craters it was also possible to obtain measurements of the height of the far rim above the surrounding terrain (Figure A1). This permits the depth of excavation of

the crater into the preexisting target to be inferred. Errors for the depth/diameter values were calculated as follows:

$$((\text{depth} + \text{error})/(\text{diameter} - \text{error}) - (\text{depth} - \text{error})/(\text{diameter} + \text{error}))/2.$$

Possible Errors: (1) Particularly for the relatively high-sun images (INA $< \sim 70°$), it is possible that the shadow of the crater wall did not fall on the flat portion of the crater floor. For simple bowl-shaped craters (typically ~4–8 km diameter; Pike, 1980), it is also possible that the shadow of the crater rim may fall on the far inner wall of the crater, particularly in low-sun images (INA $> \sim 75°$). We are able to discount this second situation because, through visual analysis of the measured craters, we excluded all craters where the shadow falls beyond the center of the parent crater.

To assess the possible occurrence of the shadow of the rim falling on the near inner wall, we have investigated the depth/diameter (d/D) ratio for the Hesperia Planum craters as a function of incidence angle (Figure A2). Somewhat surprisingly, we find that at high-sun angles (INA $< \sim 70°$), fresh craters have a higher d/D value than at lower sun angles (INA $> \sim 75°$). This is the opposite of what would be expected if the rim shadow were to fall on the nearside interior wall rather than on the crater floor: this situation should cause the crater depth to be underestimated producing a lower d/D value than should have been measured. The data (Figure A2) therefore lead us to believe that the calculated crater depths are accurate and are not affected by the illumination geometry.

References

Barlow, N. G. and Bradley, T. L.: 1990, 'Martian Impact Craters: Correlations of Ejecta and Interior Morphologies with Diameter, Latitude, and Terrain', *Icarus* **87**, 156–179.

Boyce, J. M.: 1979, 'A Method for Measuring Heat Flow in the Martian Crust Using Impact Crater Morphology', Rpts. Planet. Geol. Prog. 1978–1979, NASA TM-80339, pp. 114–118.

Carr, M. H., Crumpler, L. S., Cutts, J. A., Greeley, R., Guest, J. E., and Masursky, H.: 1977, 'Martian Impact Craters and Emplacement of Ejecta by Surface Flow', *J. Geophys. Res.* **82**, 4055–4065.

Cintala, M. J. and Mouginis-Mark, P. J.: 1980, 'Martian Fresh Crater Depths: More Evidence for Subsurface Volatiles', *Geophys. Res. Lettrs.* **7**, 329–332.

De Hon, R. A.: 1985, 'Thickness of Ridged Plains Materials in Hesperia Planum', Mars, Rpt. Plan. Geol. Prog., 1984, NASA TM-87563, pp. 242–244.

Fanale, F. P.: 1976, 'Martian Volatiles: their Degassing History and Geochemical Fate', *Icarus* **28**, 179–202.

Fanale, F. P., Salvail, J. R., Zent, A. P., and Postawko, S. E.: 1986, 'Global Distribution and Migration of Subsurface Ice on Mars', *Icarus* **67**, 1–18.

Greeley, R. and Guest J. E.: 1987, 'Geologic Map of the Eastern Equatorial Region of Mars', U.S. Geological Survey, Miscellaneous Map I-1802-B.

Hayashi-Smith, J. and Mouginis-Mark, P. J.: 1990, 'Morphology of Fresh Impact Craters in Hesperia Planum, Mars', *Lunar Planet. Sci.* **XXI**, 475–476 (abstract).

Hörtz, F., Ostertag, R. and Rainey, D. A.: 1983, 'Bunte Breccia of the Ries: Continuous Deposits of Large Impact Craters', *Revs. Geophys. Space Phys.* **21**, 1667–1725.

Kieffer, S. W. and Simonds, C. H.: 1980, 'The Role of Volatiles and Lithology in the Impact Cratering Process', *Rev. Geophys. Space Phys.* **18**, 143–181.

Mouginis-Mark, P. J.: 1979, 'Martian Fluidized Crater Morphology: Variations with Crater Size, Latitude, Altitude, and Target Material', *J. Geophys. Res.* **84**, 8011–8022.

Mouginis-Mark, P. J.: 1981, 'Ejecta Emplacement and Modes of Formation of Martian Fluidized Ejecta Craters', *Icarus* **45**, 60–76.

Pieters, C. M.: 1982, 'Copernicus Crater Central Peak: Lunar Mountain of Unique Composition', *Science* **215**, 59–61.

Pike, R. J.: 1980, 'Control of Crater Morphology by Gravity and Target Type: Mars, Earth, Moon', *Proc. Lunar Planet. Sci. Conf. 11th*, pp. 2159–2189.

Robinson, M. S.: 1990, 'Precise Topographic Measurements of Apollinaris and Tyrrhena Paterae, Mars', *Lunar Planet. Sci.* **XXI**, 1027–1028 (abstract).

Stoffler, D., Gault, D. E., Wedekind, J., and Polkowski, G.: 1975, 'Experimental Hypervelocity Impact into Quartz Sand: Distribution and Shock Metamorphism of Ejecta', *J. Geophys. Res.* **80**, 4062–4077.

Wood, C. A., Head, J. W., and Cintala, M. J.: 1978, 'Interior Morphology of Fresh Martian Craters: The Effects of Target Characteristics', *Proc. Lunar Planet. Sci. Conf., 9th*, pp. 3691–3709.

Zuber, M. T., Smith, D. E., Solomon, S. C., Muhleman, D. O., Head, J. W., Garvin, J. B., Abshire, J. B., and Bufton, J. L.: 1992, 'The Mars Observer Laser Altimeter Investigation', *J. Geophys. Res.* **97**, 7781–7797.